ELSEVIER

Nuclear Instruments and Methods in Physics Research B 168 (2000) 237–244

NIM B
Beam Interactions with Materials & Atoms

www.elsevier.nl/locate/nimb

Formation mechanism of silver nanocrystals made by ion irradiation of $Na^+ \leftrightarrow Ag^+$ ion-exchanged sodalime silicate glass

D.P. Peters, C. Strohhöfer, M.L. Brongersma, J. van der Elsken, A. Polman *

FOM-Institute for Atomic and Molecular Physics, Kruislaan 407, 1098 SJ Amsterdam, Netherlands

Received 15 March 1999; received in revised form 18 November 1999

Abstract

Sodalime silicate glass surface layers were doped with up to 7.0 at.% Ag^+ ions by ion-exchange in a $AgNO_3/NaNO_3$ solution at 330–355°C. Ion irradiation using either 400 and 500 keV He, 1 MeV Ne or 2 MeV Xe was then used to induce the growth of metallic nanocrystals in the ion-exchanged region. The ion fluences ranged from 1.3×10^{14} ions/cm^2 to 1.1×10^{17} ions/cm^2. X-ray and electron diffraction show small Ag nanocrystals with a broad size distribution, up to a diameter of 10–15 nm, after irradiation. Optical transmission measurements show the characteristic surface plasmon resonance of metallic Ag around 420 nm. The absorption resonance sharpens and increases in strength with increasing ion irradiation fluence, indicating that both nanocrystal size and volume fraction increase with irradiation fluence. Depending on ion fluence, up to ~15% of the ion-exchanged Ag^+ ions is incorporated in nanocrystals. From a systematic comparison of the degree of nanocrystal formation as a function of ion species, fluence and energy, it is concluded that nanocrystal formation is mainly caused by the atomic displacement energy loss component of the incoming ion beam; the electronic energy deposition component is less efficient.

PACS: 61.72.Ww; 81.40.Wx; 42.70.Nq; 42.79.Gn
Keywords: Ion-exchange; Ion irradiation; Energy loss; Metallic nanocrystals; Extinction

1. Introduction

The $Na^+ \leftrightarrow Ag^+$ ion-exchange technique is a well-established method to dope surface layers of sodalime silicate glass with Ag^+ ions [1]. Depending on the exchange time and temperature, Ag^+ concentrations of several at.%, extending to a depth of several microns, can be achieved. Such Ag^+-doped layers can be used as low-loss planar optical waveguides. It has been shown before that ion irradiation of these ion-exchanged waveguides with He ions causes the formation and growth of silver nanocrystals [2,3]. Metallic nanocrystals display strong non-linear optical properties [4,5], and therefore, nanocrystal doped planar waveguides may be used in all-optical switching components. As ion irradiation is a technique that can

* Corresponding author. Tel.: +31-20-6081234; fax: +31-20-6684106.
E-mail address: polman@amolf.nl (A. Polman).

0168-583X/00/$ - see front matter
PII: S0168-583X(99)00891-5

be applied locally, e.g. on a small lithographically defined area, the combination of ion-exchange to fabricate waveguides, and ion irradiations, to locally fabricate a non-linear region, seems promising for the fabrication of a planar waveguide switch.

Before pursuing such applications, it is first necessary to understand and control the details of the nanocrystal formation process, and to answer questions such as: how does the nanocrystal growth depend on ion irradiation conditions like ion energy, ion species, atomic displacement energy loss or electronic energy loss; what is the nanocrystal size distribution, and what determines the nucleation and growth kinetics?

In this paper we use 400 and 500 keV He, 1 MeV Ne, and 2 MeV Xe ion irradiation of $Na^+ \leftrightarrow Ag^+$ ion-exchanged sodalime glass at various fluences, in combination with X-ray diffraction (XRD), electron microscopy and optical extinction measurements to answer some of these questions. It is found that both the Ag nanocrystal size and volume fraction increase with irradiation fluence. For the fluence range studied, up to ~15% of the ion-exchanged Ag is incorporated in nanocrystals. Characteristic differences are found between the effect of either atomic displacement energy loss or electronic energy loss on the growth of Ag nanocrystals.

2. Experimental

Sodalime silicate glass samples of 0.6 mm thickness were ultrasonically cleaned using trichloroethylene, acetone and propanol. Next, the samples were preheated and immersed in a molten solution of 5 mol% $AgNO_3$ in $NaNO_3$ to induce $Na^+ \leftrightarrow Ag^+$ ion-exchange. Temperatures between 330°C and 355°C and exchange times between 10 and 20 min. were used. After ion-exchange a slight yellow discoloration was observed.

The ion-exchanged samples were mounted on a copper block using vacuum grease to provide good thermal contact, and irradiated with either 400 or 500 keV He, 1 MeV Ne, or 2 MeV Xe ions. Irradiation was performed at room temperature at a base pressure of 6×10^{-7} mbar. The implantation ranges were all between 1 and 2 μm, as calculated with TRIM, a Monte Carlo simulation program [6]. The fluences were varied between 1.3×10^{14} and 1.1×10^{17} ions/cm^2. The irradiation flux was kept below 7×10^{12} ions/cm^2/s in order to prevent heating effects.

Rutherford backscattering spectrometry (RBS) was performed using a 2 MeV He beam and a scattering angle of 165°, in order to determine the composition of the sodalime glass samples before and after the ion-exchange. XRD spectra were taken with a Cu $K\alpha_1$ beam ($\lambda = 0.154$ nm) using a PDS 120 Enraf-Nonius X-ray diffractometer set in powder diffraction geometry. Cross-sectional transmission electron microscopy (TEM) images were taken using a 300 kV electron beam from a Philips CM 30T electron microscope. Electron diffraction micrographs were also obtained. Optical transmission measurements were performed using the transmission setting of a spectroscopic ellipsometer with the incident beam perpendicular to the sample surface. The wavelength was scanned from 250 to 1100 nm in 2 nm steps.

3. Results and discussion

3.1. Nanocrystal characterisation

Fig. 1 shows RBS spectra of an untreated sodalime silicate glass sample and an ion-exchanged sample (355°C, 20 min.). The spectrum of the untreated sample shows the leading edges of O, Na, Si and Ca. The glass composition derived from the spectrum is (in at.%): 25 Si, 60 O, 12 Na, 3.0 Ca, and possibly small concentrations of other constituents that are below the detection limit of RBS. The spectrum of the ion-exchanged sample shows a large Ag contribution. The Ag concentration at the surface derived from this spectrum is 4.1×10^{21} Ag/cm^3, corresponding to 7.0 at.%. Taking into account the variation in energy loss and scattering cross-section with depth for RBS, it is concluded that the Ag concentration gradually decreases with depth. The maximum Ag diffusion depth is estimated to be well beyond 4 μm.

Fig. 2 shows the XRD spectrum of an ion-exchanged sample irradiated with 500 keV He to a

fluence of 1.1×10^{17} ions/cm^2. The broad band peaked around 20–25° is typical for sodalime glass. The peak at $2\theta = 38°$ is not observed in the spectrum of an ion-exchanged, non-irradiated sample (not shown). The inset in Fig. 2 shows an enlargement of this peak after a linear background subtraction. A Gaussian fit through the data is also shown. It peaks at $2\theta = 37.9°$ and has a full-width at half maximum of 0.64°. This peak can be attributed to diffraction from Ag (1 1 1) planes, with a lattice spacing of 2.36 Å. From the width, a Ag nanocrystal diameter can be estimated: it amounts to ~13 nm. Note that a small peak is also observed in the spectrum at $2\theta = 44°$, which can be attributed to scattering from Ag (2 0 0) planes.

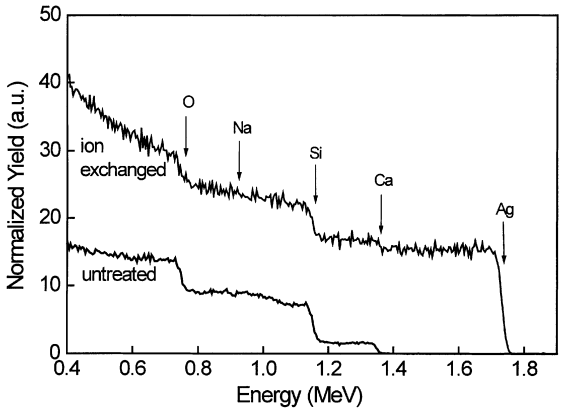

Fig. 1. RBS spectrum of an ion-exchanged sample and an untreated reference sample taken with a 2.0 MeV He beam at a scattering angle of 165°. The ion-exchanged sample was treated in a 5 mol% $AgNO_3$ solution in $NaNO_3$ for 20 min at 355°C. The surface energies for the various constituents are indicated.

Fig. 3 shows a cross-sectional dark-field TEM micrograph of the same sample as in Fig. 2. The image was taken at a depth of ~1 μm using diffraction from the Ag (1 1 1) planes. The inset in Fig. 3 shows an electron diffraction micrograph taken from the same region. The TEM image clearly shows the presence of spherical nanocrystals with a maximum diameter of ~10–15 nm. The majority of the nanocrystals have much smaller radii, down to at least 3.5 nm, the image resolution. The diffraction pattern in the inset of Fig. 3 shows three clear rings, which can be assigned to Ag (1 1 1), (2 0 0) and (2 2 0) planes. No texture or preferential orientation of the nanocrystals is observed. Using similar cross-sectional TEM images taken at different distances from the sample surface (not shown), one can observe the density of

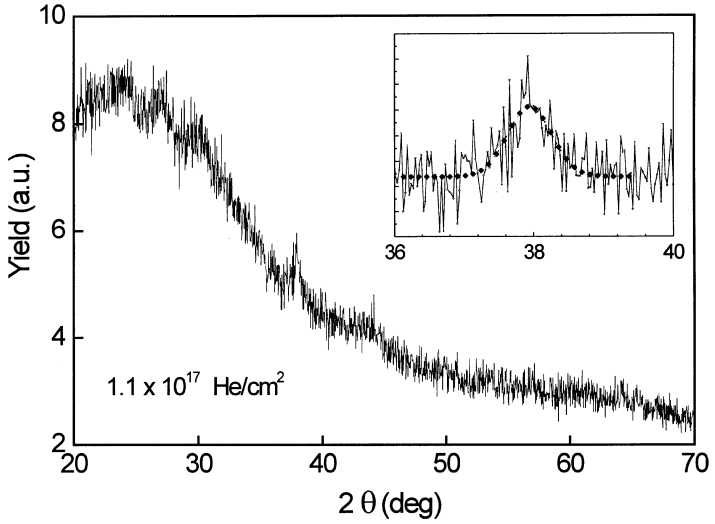

Fig. 2. X-ray diffraction spectrum of an ion-exchanged sample, irradiated with 1.1×10^{17} 500 keV He ions/cm^2. Ion exchange parameters were identical to those for the sample of Fig. 1. The spectrum was taken with a beam of Cu Kα_1 radiation ($\lambda = 0.154$ nm). The inset shows an enlargement of the Ag (1 1 1) peak after background subtraction, together with a fit from which an average nanocrystal size of ~13 nm was estimated.

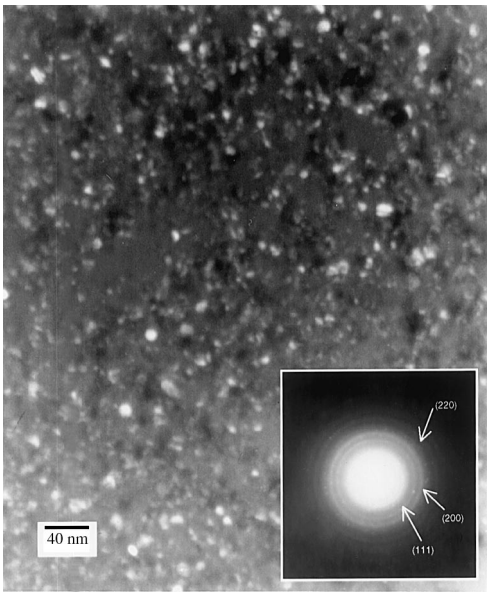

Fig. 3. Cross-sectional TEM dark field image for the Ag (1 1 1) orientation, for the same sample as in Fig. 2, taken at a depth of 1 μm from the sample surface. The inset shows the diffraction micrograph in which the rings for Ag (1 1 1), (2 0 0) and (2 2 0) planes are visible.

nanocrystals to decrease with depth. No Ag nanocrystals are found at a depth of 4 μm, well beyond the range of 500 keV He.

Fig. 4(a) shows optical transmission spectra of ion-exchanged samples irradiated with 400 keV He to fluences of 1.1×10^{16}, 2.6×10^{16} and 8.1×10^{16} ions/cm^2, as well as the spectra of a sodalime glass reference sample (indicated by *r*) and an ion-exchanged, non-irradiated sample (indicated by 0). All transmission spectra display a transmission cut-off below 300 nm due to the absorption of the glass substrate. For the untreated glass sample a transmission of 88% is observed over the full spectral range from 310 to 1100 nm. As can be seen in Fig. 4(a), ion-exchange causes a slight decrease in transmission over the entire spectral range. The subsequent ion irradiation causes a further decrease in transmission over the whole wavelength range from 300 to 1100 nm. For increasing irradiation fluences a transmission dip evolves, centred at ~420 nm. For the highest irradiation fluence the minimum transmission at $\lambda = 418$ nm is only 2%.

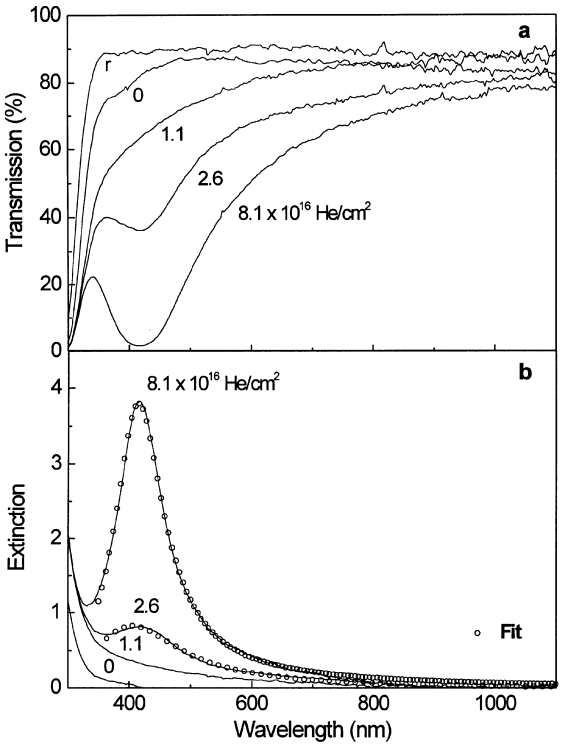

Fig. 4. (a) Optical transmission spectra of ion-exchanged samples irradiated with 400 keV He up to fluences of 1.1×10^{16}, 2.6×10^{16} and 8.1×10^{16}ions/cm^2. "*r*" indicates the spectrum of an untreated reference sample, "0" indicates the spectrum of an ion-exchanged, non-irradiated sample. (b) Extinction spectra of the samples in Fig. 4(a), obtained from the transmission spectra as explained in the text. The open circles represent fits using Mie theory (Eq. (1)), from which the nanocrystal diameter and volume of metallic Ag per unit area were estimated.

Fig. 4(b) shows extinction spectra obtained from the data in Fig. 4(a), using the transmission of the untreated glass sample at $\lambda = 1000$ nm as a reference. These extinction spectra $E(\lambda)$ can be compared to the well-known Mie theory for the extinction of a metallic nanocrystal composite [7]. For nanocrystal sizes below 20 nm, optical scattering contributions are negligible, and only the electric dipole term in the Mie expression has to be taken into account [8],

$$E(\lambda) = 18\pi f \varepsilon_m^{3/2} \frac{\varepsilon_2}{\lambda\left((\varepsilon_1 + 2\varepsilon_m)^2 + \varepsilon_2^2\right)}, \qquad (1)$$

with

$$\varepsilon_1 = \varepsilon_1'(\omega) + 1 - \frac{\omega_p^2}{\omega^2 + \omega_c^2},$$

$$\varepsilon_2 = \varepsilon_2'(\omega) + \frac{\omega_p^2 \omega_c}{\omega} \frac{1}{\omega^2 + \omega_c^2}, \qquad \omega_c = \frac{v_f}{l} + \frac{2v_f}{d},$$

where $\omega = 2\pi c/\lambda$, λ the wavelength in vacuum and c the speed of light in vacuum. ε_m is the effective dielectric constant of the matrix and f the volume of metallic Ag per unit area of the irradiated layer. ε_1 and ε_2 are the real and imaginary part of the dielectric function of the nanocrystal, respectively, and $\varepsilon_1'(\omega)$ and $\varepsilon_2'(\omega)$ the real and imaginary parts of the frequency dependent dielectric function of bulk Ag due to interband transitions [9]. ω_p is the plasma frequency of silver, v_f the Fermi velocity of electrons in bulk Ag, l the electron mean free path in bulk Ag and d the diameter of the Ag nanocrystals.

Fitting Eq. (1) to the data for the two highest fluences in Fig. 4(b), using literature values [10] of $v_f = 1.38 \times 10^6$ m/s, $l = 57$ nm and $\omega_p = 1.37 \times 10^{16}/s^1$ and taking f, d and ε_m as fitting parameters yields the open circle data in Fig. 4(b): the fits show excellent agreement with the experimental data. Note that we used a single nanocrystal diameter d in the fitting procedure. Fits obtained using a discrete nanocrystal size distribution indicate that the nanocrystal diameter d is sharply peaked around a central value, with a standard deviation of less than 1 nm. Taking a larger standard deviation in d increases the error of the fit considerably. Therefore we believe the use of a single nanocrystal diameter to be justified.

Comparing the data for the different fluences in Fig. 4(b) it can be seen that the absorption resonance sharpens and increases in strength with increasing irradiation fluence. This implies that the nanocrystal size and volume fraction increase with fluence. Table 1 shows the values of d and f as extracted from the fits shown in Fig. 4(b). Also shown is the fraction of metallic Ag, obtained by dividing f by the ion range and taking into account the density of Ag and the surrounding matrix. Data are also shown for ion-exchanged samples irradiated with 1 MeV Ne and 2 MeV Xe at various fluences. For these irradiations too, the nanocrystal size and volume fraction increase with fluence. Comparing the calculated fraction of metallic Ag in Table 1 with the Ag concentration in the ion irradiated region (7.0 at.% at the surface, gradually decreasing with depth), the fraction of ion-exchanged Ag^+ that is incorporated into Ag nanocrystals can be estimated. For the highest fluence irradiation (400 keV He, $8.1 \times 10^{16}/cm^2$), it amounts to roughly ~15%.

It should be noted that the spectrum for the lowest irradiation fluence in Fig. 4(b) does not show a characteristic resonance peak. This may indicate that the sample contains a large density of very small nanocrystals. Alternatively, it could be that the measured extinction for low fluence irradiation is due to other sources than nanocrystals, e.g. ion irradiation-induced defects. In the latter case the extinction data for the higher fluences should be corrected for this background. Fitting the data for the two highest irradiation fluences in Fig. 4(b) after subtraction of a smooth background yields different values for the fit parameters, as shown between brackets in Table 1.

Comparing the data from the XRD, TEM and extinction measurements for the high fluence He irradiation, it can be seen that three different typical nanocrystal diameters have been found. The largest nanocrystals found using XRD (Fig. 2) have a diameter of ~13 nm, which is in agreement with the TEM data (Fig. 3), from which a maximum diameter ~10–15 nm is found. Note that mainly large nanocrystals will contribute to peaks in the X-ray spectrum, as smaller nanocrystals yield flat, broad peaks that cannot be detected. The TEM image also clearly shows that the majority of nanocrystals have radii of ~5 nm and smaller. This is in good agreement with the extinction spectrum (Fig. 4(b)), which yields an average nanocrystal diameter of 2.2 nm. Note for reference that a Ag nanocrystal of this size contains roughly 600 Ag atoms.

Measurements of the non-linear properties of these ion-irradiation-induced Ag nanocrystals have been performed using the Z-scan technique. Preliminary data show that the refractive index shows a large negative electronic non-linearity and a positive thermal contribution [11]. In addition, a non-linear absorption is found. These data

Table 1
Nanocrystal diameter d, volume of metallic Ag per unit area f, and fraction of metallic Ag, obtained from fits to the extinction data for 400 keV He, 1 MeV Ne and 2 MeV Xe irradiation using Eq. (1)[a]

Ion	Irradiation fluence (ions/cm^2)	Diameter d (nm)	f (nm)	Fraction of metallic Ag (at.%)
400 keV He	2.6×10^{16}	1.3 (1.6)	6.0 (0.4)	0.31 (0.18)
	8.1×10^{16}	2.2 (2.6)	17.1 (13.5)	0.90 (0.72)
1 MeV Ne	1.7×10^{15}	1.3 (–)	3.7 (–)	0.28 (–)
	3.9×10^{15}	1.4 (2.1)	4.8 (1.4)	0.35 (0.09)
	5.4×10^{15}	1.4 (2.3)	5.2 (1.4)	0.38 (0.09)
2 MeV Xe	5.0×10^{14}	1.3 (2.0)	5.0 (0.9)	0.21 (0.09)
	1.1×10^{15}	1.6 (2.2)	4.3 (1.2)	0.41 (0.10)
	2.0×10^{15}	1.8 (2.2)	5.6 (3.6)	0.54 (0.35)

[a] The value between brackets was obtained from fits after a smooth background subtraction to the extinction curves had been performed.

indicate that these irradiation-induced Ag nanocrystals may indeed be used in all-optical switching applications.

3.2. Nanocrystal formation mechanism: electronic versus atomic displacement energy loss

Fig. 5 shows the measured extinction at $\lambda = 418$ nm as a function of the irradiation fluence for 400 keV He, 1 MeV Ne and 2 MeV Xe irradiated samples. For all three irradiation conditions the extinction increases with fluence. However, the fluence to reach a particular extinction depends on the ion/energy condition used: the extinction per Xe ion is larger than for Ne, and for Ne the increase is larger than for He. The inset shows the integrated energy deposition in electronic excitations and in atomic displacements for the three irradiation conditions, calculated using TRIM. As can be seen, for all three ion species the largest fraction of the ion energy is deposited in electronic interactions. For the three ion/energy conditions used, the integrated electronic energy loss varies by less than a factor 3, while the energy lost in atomic displacements varies by more than a factor 50. Comparing the trends in the inset with the data for the three different ions, it appears that the nanocrystal formation efficiency trend found in the data is best represented by the trend in the atomic displacement calculation.

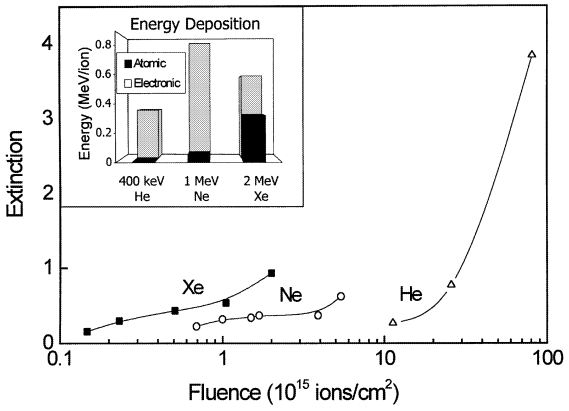

Fig. 5. Extinction at $\lambda = 418$ nm as a function of irradiation fluence, for ion-exchanged samples irradiated with 400 keV He (△), 1 MeV Ne (○) and 2 MeV Xe (■). The inset shows the integrated energy deposited in atomic displacements and electronic excitations, as calculated using TRIM.

To further investigate this, the extinction data in Fig. 5 were normalized to the integrated amount of energy loss deposited in atomic displacements. These data are shown in Fig. 6. For all ion species, the extinction shows the same initial increase as a function of deposited energy. For higher energy deposition values, the Ne and Xe data follow the same trend shown by the drawn line, while the data for He diverges sharply (dashed line). The difference between the results for He on the one hand and the heavy ions (Ne, Xe)

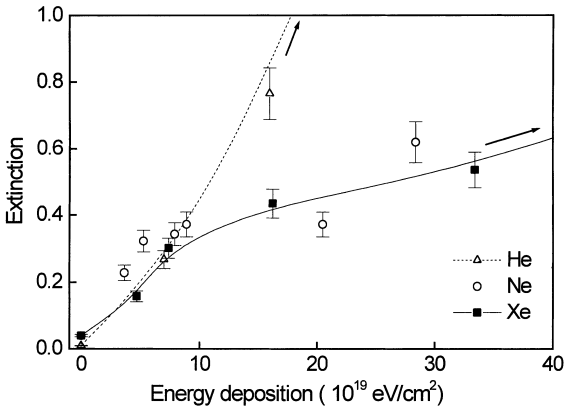

Fig. 6. Extinction at $\lambda = 418$ nm as a function of irradiation fluence normalized to atomic displacement energy loss for the same samples as in Fig. 5: He (△), Ne (○) and Xe (■). The lines are a guide to the eye and arrows indicate the position of additional data points for He and Xe outside the range of the graph.

on the other hand, may be due to the fact that only a very small fraction of the stopping for He is due to atomic displacement energy loss. The trends in Fig. 6 may be understood if it is assumed that nanocrystal formation may also be caused by electronic energy loss, though much less efficiently than by atomic displacements, and that both these processes have a different dependence on fluence. Indeed, it may be that both energy loss processes have a distinctly different effect on the nucleation and growth kinetics of nanocrystals. More measurements are needed to investigate this in more detail.

The conclusion that atomic displacement energy loss is the main factor responsible for nanocrystal nucleation seems in contradiction with data on the effect of light ion irradiation on nanocrystal formation in [2]. However, in the experiments in that reference, the atomic displacement energy loss component was very small, and therefore the effect of electronic energy loss may have become apparent. Indeed, our data above show that the nanocrystal formation rate during He irradiation is much smaller than during heavy ion irradiation. Recently, a paper has been published by Ila et al. [12], in which it was reported that electronic energy loss caused the growth of Au nanocrystals from an irradiated region containing pre-implanted Au ions. It is difficult to compare these data with those in the present paper, as beam-induced effects of the Au implantation itself can cause nucleation of (small, possible undetectable) nanocrystals during ion irradiation. In contrast, in our experiments, the incorporation of the Ag ions by ion-exchange and the ion irradiation are two independent processes.

4. Conclusions

Ag nanocrystals were formed by 400 and 500 keV He, 1 MeV Ne and 2 MeV Xe irradiation of $Na^+ \leftrightarrow Ag^+$ ion-exchanged sodalime glass. The nanocrystal size and volume fraction increase with ion fluence. For a 500 keV, 1.1×10^{17} ions/cm^2 He irradiation, a broad nanocrystal size distribution is found, with diameters up to 10–15 nm. Up to ~15% of the ion-exchanged Ag ions is incorporated in nanocrystals. Comparing the extinction spectra for various irradiation conditions it is concluded that for Ne and Xe irradiation nanocrystals are most efficiently formed by the effect of the energy deposited in atomic displacement collisions. For He, an electronic energy deposition component may also play a role. Both kinds of energy deposition may have a different effect on the nucleation and growth of nanocrystals. These Ag nanocrystal doped ion-exchanged layers may serve as non-linear waveguides for use in planar all-optical switching components.

Acknowledgements

This work is part of the research program of the "Stichting voor Fundamenteel Onderzoek der Materie (FOM)", which is financially supported by the "Nederlandse organisatie voor Wetenschappelijk Onderzoek (NWO)". We gratefully acknowledge the help of René Koper for TEM sample preparation, Hennie Zandbergen (TU Delft) for cross-section TEM measurements and analysis, and Bert Moleman (UvA) for XRD measurements.

References

[1] R.V. Ramaswamy, R. Srivastava, J. Lightwave Technol. 6 (1988) 984.
[2] F. Caccavale, G. De Marchi, F. Gonella, P. Mazzoldi, G. Meneghini, A. Quaranta, G.W. Arnold, G. Battaglin, G. Mattei, Nucl. Instr. and Meth. B 96 (1995) 382.
[3] G. De Marchi, F. Gonella, P. Mazzoldi, G. Battaglin, E.J. Knystautas, C. Meneghini, J. Non-Cryst. Solids 196 (1996) 79.
[4] F. Hache, D. Ricard, C. Flytzanis, J. Opt. Soc. Am. B 3 (1986) 1647.
[5] G.W. Arnold, G. De Marchi, F. Gonella, P. Mazzoldi, A. Quaranta, G. Battaglin, M. Catalano, F. Garrido, R.F. Haglund Jr., Nucl. Instr. and Meth. B 116 (1996) 507.
[6] J.F. Ziegler, J.P. Biersack, U. Littmark, The Stopping and Range of Ions in Solids, Pergamon, New York, 1985.
[7] G. Mie, Ann. Physik (Leipzig) 25 (1908) 377.
[8] G.W. Arnold, J.A. Borders, J. Appl. Phys. 48 (1977) 1488.
[9] P.B. Johnson, R.W. Christy, Phys. Rev. B 6 (1972) 4370.
[10] R.W. Ashcroft, N.D. Mermin, Solid State Physics, Saunders College, Philadelphia, 1976.
[11] D.P. Peters, Silver nanocrystals in sodalime glass, Master thesis, FOM-Institute for Atomic and Molecular Physics, 1998.
[12] D. Ila, E.K. Williams, C.C. Smith, D.P. Poker, D.K. Hensley, C. Klatt, S. Kalbitzer, Nucl. Instr. and Meth. B 148 (1999) 1012.